photonics

Communication

Look-Up-Table-Based Direct-Detection-Faster-Than-Nyquist-Algorithm-Enabled IM/DD Transmission with Severe Bandwidth Limitation

Xiaoying Zhang, Jiahao Huo *, Shaonan Liu, Wei Huangfu and Keping Long

Beijing Engineering and Technology Research Center for Convergence Networks and Ubiquitous Services, University of Science and Technology Beijing, Beijing 100083, China; d202210375@xs.ustb.edu.cn (X.Z.); m202120764@xs.ustb.edu.cn (S.L.); huangfuwei@ustb.edu.cn (W.H.); longkeping@ustb.edu.cn (K.L.)
* Correspondence: huojiahao@ustb.edu.cn

Abstract: The emergence of new applications is driving a dramatic growth in the capacity of data center interconnects. Intensity modulation and direct detection (IM/DD) has the characteristics of low cost, low power consumption and a small footprint. Industry and academia have conducted much research on IM/DD systems as a cost-effective solution. However, optical/electronic bandwidth and fiber dispersion are the restricting factors for the improvement of transmission capacity. Pattern-dependent distortion is an important aspect that affects system performance. In this paper, we propose a look-up table (LUT)-based direct-detection-faster-than-Nyquist (DDFTN) algorithm to compensate for pattern-dependent distortion. The performances of feedforward-equalization (FFE) only, the original DDFTN, least-squares (LS)-based DDFTN, and LUT-based DDFTN algorithms in IM/DD-based 112/140 Gbit/s four-level pulse-amplitude modulation (PAM-4) signal transmission were evaluated. The experimental results indicate that LUT-based DDFTN performs better with low computational complexity.

Keywords: intensity modulation and direct detection (IM/DD); four-level pulse-amplitude modulation (PAM-4); look-up table (LUT); direct detection faster than Nyquist (DDFTN)

Citation: Zhang, X.; Huo, J.; Liu, S.; Huangfu, W.; Long, K. Look-Up-Table-Based Direct-Detection-Faster-Than-Nyquist-Algorithm-Enabled IM/DD Transmission with Severe Bandwidth Limitation. *Photonics* **2023**, *10*, 1222. https://doi.org/10.3390/photonics10111222

Received: 14 September 2023
Revised: 13 October 2023
Accepted: 26 October 2023
Published: 31 October 2023

1. Introduction

The requirement for high-capacity services is continuously increasing. The intensity modulation and direct detection (IM/DD) optical system has been investigated extensively in short-reach applications due to its advantage in cost and power consumption. Although advanced modulation techniques increase the data rate, non-return-to-zero on–off keying (NRZ-OOK) [1] and four-level pulse-amplitude modulation (PAM-4) [2,3] are the preferred choice for IM/DD systems.

The transmission capacity of IM/DD systems is limited by the optical/electronic bandwidth and the fiber dispersion. Inter-symbol interference (ISI) is introduced and decreases the system performance due to band-limited devices and chromatic dispersion (CD)-induced power fading. Digital signal processing (DSP) algorithms have been introduced to mitigate the ISI, such as the feedforward equalizer (FFE) [4], decision feedback equalizer (DFE) [5], and maximum-likelihood sequence estimation (MLSE) algorithms [6]. However, the FFE algorithm aggravates in-band high-frequency noise and DFE causes error propagation. Prior studies demonstrate the superiority of the direct-detection-faster-than-Nyquist (DDFTN) algorithm, which combines matched filtering and subsequent MLSE [7–12]. At the 7% hard-decision forward-error correction (HD-FEC) threshold, the 140 Gbit/s PAM-4 under-20 km standard single-mode fiber (SSMF) transmission in the O band was investigated using the MLSE algorithm [13]. In the original DDFTN, the calculation of the estimated symbol depends on the tap coefficients of the postfilter. The least-squares (LS) channel estimation process was added after the postfilter in prior studies and was shown to perform better [14–16]. The MLSE is superior in solving pattern-dependent ISI. However, the computational complexity of applying MLSE lies in the Viterbi algorithm and increases exponentially with the memory length. The ultra-high computational complexity limits its hardware implementation [17]. The look-up table (LUT) not only can be very effective in solving signals with pattern-dependent distortions but also has lower computational complexity.

The LUT-based method associates the symbol error with its neighboring symbols and has been investigated in recent years [18–21]. An almost 4 dB gain was achieved by adopting LUT and pre-chromatic dispersion compensation in [22]. Over 12 dB receiver sensitivity was obtained with the combination of pre-equalizer and LUT in [23]. LUT is an efficient scheme to mitigate the pattern-dependent distortion. Meanwhile, trellis-compression MLSE (TC-MLSE) equalizer has been proposed and used in IM/DD transmission systems [24,25]. Inspired by the effectiveness of LUT, we propose the LUT-based DDFTN algorithm.

In this paper, we use the C band IM/DD system to experimentally demonstrate 112 and 140 Gbit/s PAM-4 transmission under back-to-back (BTB) and 2/1 km SSMF. Compared with the original DDFTN and LS-based DDFTN, the LUT-based DDFTN can evidently improve the performance with lower computational complexity. The operation principle of the original DDFTN, LS-based DDFTN, and LUT-based DDFTN algorithms are introduced in Section 2. The computational complexity between the LS-based DDFTN and LUT-based DDFTN algorithm is also analyzed. In Section 3, we provide a detailed description of the experimental setup. In Section 4, we investigate the performance of the system with different DSP algorithms. In Section 5, we conclude this paper.

2. Principle

Advanced DSP is necessary to mitigate ISI in IM/DD transmission. Among these, DDFTN has been widely investigated in recent years. DDFTN combines matched filtering and a subsequent MLSE. Firstly, the received symbol processed by the FFE is fed into the postfilter. Secondly, various methods can be used to obtain the estimated symbol. Then, the error between the estimated symbol and the output symbol of the postfilter can be calculated. Thirdly, accumulated error is computed in the Viterbi algorithm, and the most probable path can be obtained. A detailed description follows.

After the FFE operation, the system performance is affected by enhanced high-frequency noise. Thus, the postfilter, which can be expressed as $H(z) = 1 + \alpha z^{-1}$, is introduced. Therein, the postfilter coefficients are $(1, \alpha)$. Then, the received signal becomes

$$y(i) = S(i) + \alpha \cdot S(i-1) \tag{1}$$

where S denotes the symbol sequence from the FFE output.

In the Viterbi algorithm, the surviving path, Euclidean distance, and the most probable path are worthy of mention. The surviving path takes the pre-symbol and the post-symbol of the current estimated symbol into consideration. Taking PAM-4 with a three-symbol memory length, for example, the current estimated symbol has 16 surviving paths. Moreover, every surviving path corresponds to a value of Euclidean distance. The Viterbi algorithm can find the minimum value of the Euclidean distance and put the corresponding symbol into the most probable path. The calculation of Euclidean distance can be expressed as

$$d_i = d_{i-1} + (y(i) - ES(i))^2 \tag{2}$$

where ES is the estimated symbol, d is the accumulated Euclidean distance, and y is the output symbol of the postfilter. Moreover, the error between the estimated symbol and the output symbol of the postfilter has various expressions, which can be obtained through the original DDFTN, LS-based DDFTN, and LUT-based DDFTN.

2.1. The Original DDFTN Algorithm

Figure 1 shows the block diagram of the original DDFTN. As mentioned above, the postfilter is used after the FFE operation, and then the postfilter coefficients are further utilized in the MLSE. In the original DDFTN algorithm, the estimated signal can be obtained from the following expression:

$$ES(i) = x_i \cdot 1 + x_{i+1} \cdot \alpha \tag{3}$$

where x represents the four ideal values of PAM-4 (-3, -1, 1, and 3). However, the channel information from the postfilter is inaccurate. Influenced by the inaccurate estimated signal, the system's BER will increase.

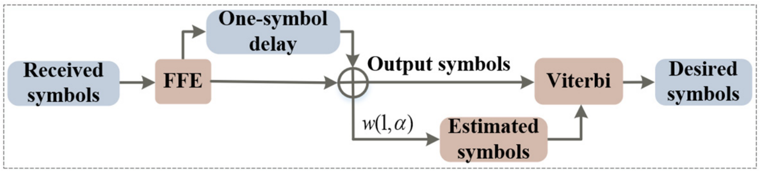

Figure 1. Block diagram of the original DDFTN.

2.2. LS-Based DDFTN Algorithm

To enhance the accuracy of the channel information, an LS channel estimator is introduced, as shown in Figure 2. In this way, the weight coefficients utilized in MLSE are closer to the actual channel situation. Then, the estimated signal is represented as

$$ES(i) = x_{i-n} \cdot w(i-n) + \ldots x_i \cdot w(i) + x_{i+1} \cdot w(i+1) + \ldots x_{i+n} \cdot w(i+n) \tag{4}$$

in which w is the weight coefficient, which can be represented as

$$w = \left(q^T q\right)^{-1} q^T y \tag{5}$$

where q is the Toeplitz matrix, which can be given by

$$q = \begin{pmatrix} b_0 & \cdots & b_{2*k+1} \\ \vdots & \ddots & \vdots \\ b_L & \cdots & b_{L-2*k-1} \end{pmatrix} \tag{6}$$

in which the length of transmitted training sequence b is L. As for the MLSE, the memory length can be expressed by $2k + 1$.

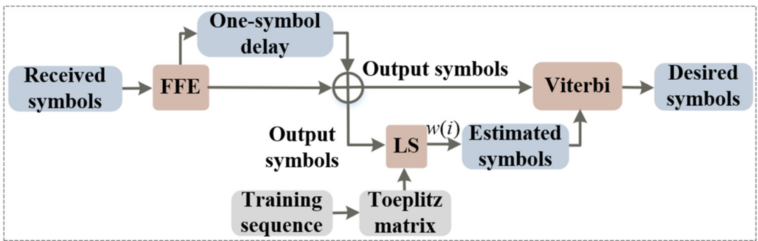

Figure 2. Block diagram of the LS-based DDFTN.

2.3. LUT-Based DDFTN Algorithm

The block diagram of the LUT-based DDFTN is illustrated in Figure 3. After the output symbols of the postfilter are obtained, the error between the output symbols and the training symbols can be calculated. Then, the error can be used to generate an error table that can record the error of the central symbol in a symbol pattern. As for the error table, the training symbols firstly generate different symbol patterns, which are represented as

$S(n-k):S(n):S(n+k)$, corresponding to different i indices. Secondly, the error related to the symbol pattern can be stored in the LUT. Meanwhile, the NT record the number of each pattern indexed by i. Lastly, the average of the LUT is operated to enhance the robust and reduce the noise influence.

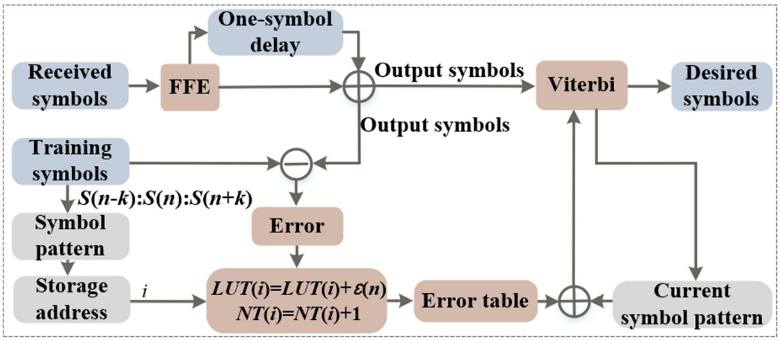

Figure 3. Block diagram of the LUT-based DDFTN.

During the execution of the Viterbi algorithm, the symbol pattern of the current symbol and the k symbols before and after are considered. Then, the Euclidean distance can be obtained by retrieving the LUT. This omits the real multiplications and real additions used in the LS algorithm, thus reducing the computational complexity. The detailed complexity analysis is as follows:

2.4. Computational Complexity Comparison

Computational complexity is an important consideration in the implementation process. The computational complexity analysis of the different DDFTN algorithms is shown in Table 1. DDFTN is related to the Viterbi algorithm. As for the PAM-M signal, where M denotes the alphabet size, M^{k+1} possible paths can be obtained while searching the surviving path. Therein, $2k+1$ denotes the channel memory length. The computational complexity of the Euclidean distance is also important. For the LS-based DDFTN, calculation of the estimated signal is associated with the value of $2k+1$ and the value of L, which represents the length of the training sequence. Thus, it requires $(2k+1)(2L+1)L$ real multiplications (RMs) and $4kL^2-(2k+1)(L-1)$ real additions (RAs). As for the LUT-based DDFTN, the expression of the estimated signal can be represented by the sum of the current symbol pattern and the LUT with M^{2k+1} addresses. The estimated signal is then obtained through searching the error table. Then, the complexity of the calculation of the estimated signal $ES(i)$ can be reduced significantly.

Table 1. Computational complexity analysis of different DDFTN algorithms.

Algorithm	RM	RA
LS-based DDFTN	$(2k+1)(2L+1)L+2(k+1)4^{k+1}$	$4kL^2-(2k+1)(L-1)+2(k+1)4^{k+1}$
LUT-based DDFTN	$2(k+1)4^{k+1}$	$2+2(k+1)4^{k+1}$

2.5. Process Analysis of Different DDFTN Algorithms

In order to help readers further understand the principle of the DDFTN algorithm, we organized a detailed analysis of the key symbol values in the DDFTN algorithm, as shown in Table 2. The experimental results of the 140 Gbit/s signal under 1 km SSMF at −1 dBm is selected for discussion (the detailed experimental setup is available in Section 3). The true symbol represents the ideal transmitted symbol. The value α of the postfilter is set at 0.6. The estimated symbol of the original DDFTN is obtained by Equation (3), where x represents the four ideal values of PAM-4 (−3, −1, 1, and 3) in decision symbols. Therefore, the estimated symbol of Symbol 1 can be verified through $-3+1\times0.6$, and the estimated symbol of Symbol 4 can be verified through $1+(-1)\times0.6$. It should be noted that there are several values of estimated symbols in the process of the DDFTN algorithm. However, only one decision symbol is obtained in the most probable path. The estimated symbol in Table 2 is the value corresponding to the most probable path.

Table 2. Process analysis of different DDFTN algorithms.

Symbol ID	**1**	**2**	**3**	**4**	**5**	**6**	**7**	**8**
True symbol	−3	3	1	3	−3	3	−3	−3
Postfilter output ($\alpha = 0.6$)	−1.29	3.05	3.13	0.89	−0.31	1.14	−3.23	−4.8
Estimated symbol of original DDFTN	−2.4	2.8	3.6	0.4	−0.4	0.4	−2.8	−4.8
Decision symbol of original DDFTN	−3	1	3	1	−1	1	−1	−3
True or false	True	False	False	False	False	False	False	True
Estimated symbol of LUT-based DDFTN (k = 1)	−1.17	3.17	2.95	1.09	−1.02	2.24	−2.69	−4.97
Decision symbol of LUT-based DDFTN (k = 1)	−3	3	1	3	−3	3	−1	−3
True or false	True	True	True	True	True	True	False	True

As we mentioned in principle, the process of obtaining the decision symbol is related to the value of the Euclidean distance. To go a step further, the smaller the difference value between the estimated symbol and the postfilter output, the smaller the Euclidean distance that is likely to be obtained. The estimated signal in the table is obtained by the original DDFTN and LUT-based DDFTN respectively satisfying the condition of the minimum Euclidean distance. It is obvious that the estimated symbol obtained by the LUT-based DDFTN method is closer to the true symbol. For example, 2.95 is much closer to 1 compared with the value of 3.6 for Symbol 3. Similarly, 1.09 is much closer to 3 compared with the value of 0.4 for Symbol 4. Therefore, the decision symbol is more likely to be consistent with the true symbol, which indicates the possibility of better performance. This can also be verified in the accuracy rate. It is obvious to see from the decision symbols that the LUT-based DDFTN has the advantage in terms of accuracy.

3. Experimental Setup

Figure 4 shows the experimental setup and DSP flow of the IM/DD PAM-4 system. At the transmitter side, a pseudorandom binary sequence (PRBS) with a length of $2^{16} - 1$ is used for PAM-4 mapping. Next, the PAM-4 sequence would be pre-emphasized and up-sampled. Then, the transmitted signal is generated, and an electrical amplifier (EA) (SHF 807) is further devoted to amplifying the PAM-4 signal. We use an arbitrary waveform generator (AWG) (Keysight M8196A) and a linear EA to drive the Mach–Zehnder modulator (MZM) (FTM7937). A standard single-mode fiber (SSMF) is placed after the MZM. When it comes to the receiver side, a variable optical attenuator (VOA) is used to adjust the received optical power (ROP) before launching the received symbol into the PD (FINISAR XPDV2120ra). Then the PD output signal is analog-to-digital converted and stored using a 33 GHz real-time oscilloscope (RTO) (UXR0334A). As for the receiver DSP, normalization and resampling is first performed. To cope with the ISI caused from bandwidth constraints and the CD effect, the FFE and the MLSE equalizer are applied. Finally, the PAM-4 signal is demapped, and we can calculate the BER.

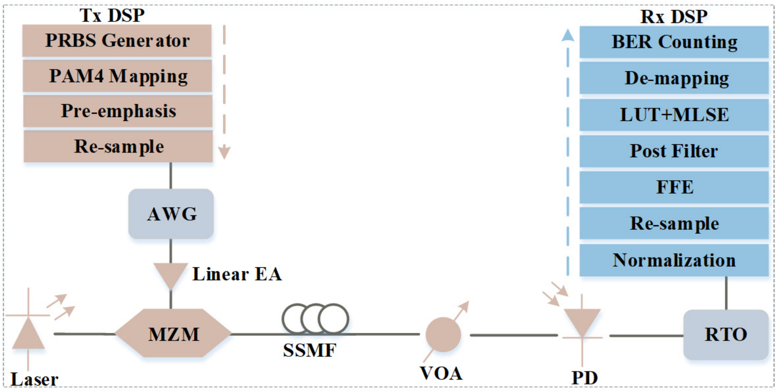

Figure 4. Experimental setup and DSP flow for the IM/DD system.

4. Results and Discussion

In this section, the LUT-based DDFTN algorithm is experimentally investigated, along with the original DDFTN and the LS-based DDFTN algorithms for comparison. Implementation of 112 Gbit/s BTB, 112 Gbit/s 2 km, 140 Gbit/s BTB, and 1 km IM/DD PAM-4 transmission experiments are carried out to demonstrate the performance of the LUT-based DDFTN. LUT-based DDFTNs with a 3-symbol pattern and a 5-symbol pattern are considered for comparison.

Firstly, 112/140 Gbit/s PAM-4 experiments under optical BTB and 2/1 km SSMF transmission are investigated. Since the postfilter affects the system performance, we optimize the α of the postfilter, as shown in Figure 5. The ROP for the 112 Gbit/s BTB, 112 Gbit/s 2 km, 140 Gbit/s BTB, and 1 km is set at -6 dBm, −3 dBm, −3 dBm, and −2 dBm, respectively. The BER can be optimized around the value of 3.8×10^{-3} by adjusting the α at the pre-set ROP. The value of α adds either constructively or destructively to the signal. The reason for this is the decreased in-band noise and the increased ISI in the meantime. As we can see from the results, the optimal value for the 112 Gbit/s signal is 0.1/0.6, and the optimal value for the 140 Gbit/s signal is found to be 0.4/0.6. In the 140 Gbit/s transmission system, α is usually larger than that in the 112 Gbit/s transmission system because of the larger ISI in the higher-speed system. Meanwhile, α is larger under the SSMF transmission compared with the BTB condition due to the effect of CD.

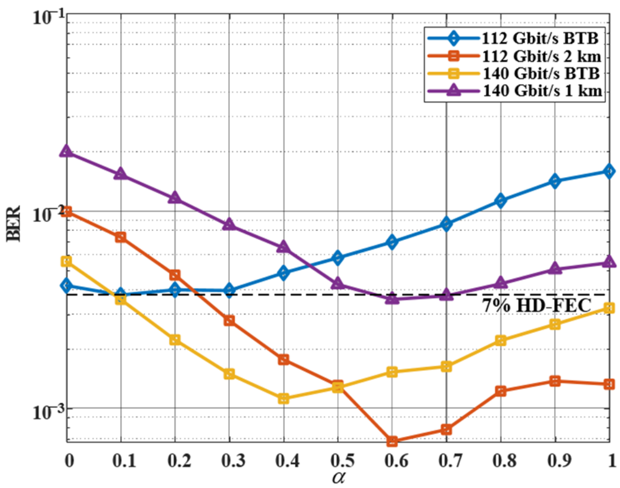

Figure 5. BER versus α for the 112 Gbit/s and the 140 Gbit/s PAM-4.

We demonstrated the performance of the LUT-based DDFTN algorithm experimentally in the 112 Gbit/s IM/DD PAM-4 transmission. In the measurements, we set α at the optimal value in Figure 5. Figure 6 presents the BER versus ROP for the considered schemes in the BTB configuration and the 2 km SSMF. The FFE algorithm and the original DDFTN algorithm are used to compare the performance to verify the validity of the LUT-based DDFTN algorithm. A similar performance tendency is observed both in the BTB and the 2 km SSMF length configurations. The four schemes have similar performances when the ROP is increased from −8 to −4 under the BTB transmission. As a result of its ability to alleviate the residual ISI, the performance of DDFTN improves as the ROP continues to increase. It is worth mentioning that 1 km SSMF in the C band has a greater effect on fiber dispersion than the optical BTB transmission; thus, it shows the worse scenario. For BTB transmission, the four schemes achieve an optical power sensitivity of approximately −5 dBm at the BER of 3.8×10^{-3}. As for the 1 km SSMF transmission, the LUT-based DDFTN exhibits about a 1.5 dB penalty in contrast with the optical BTB transmission, owing to the impact of fiber dispersion. Meanwhile, as we can see, the application of DDFTN provides over 3 dB of optical power sensitivity gain. Compared with the original DDFTN, the performance of the LUT-based DDFTN is only slightly improved.

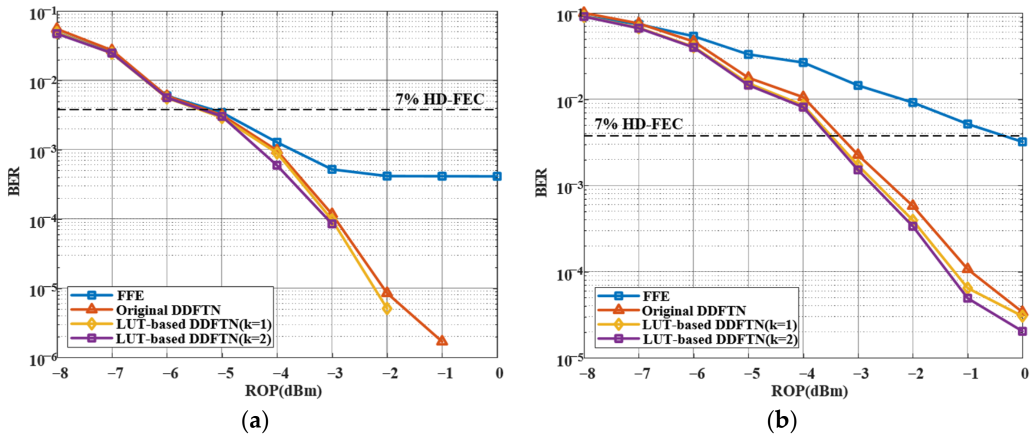

Figure 6. BER versus ROP for 112 Gbit/s PAM-4 for (**a**) BTB and (**b**) 2 km SSMF.

As for the 140 Gbit/s PAM-4, the BER versus ROP for both the BTB and the 1 km SSMF is investigated. As shown in Figure 7, BER performance deteriorates as the ROP is reduced. It clearly shows that a sensitivity of approximately −3 dBm is achievable with the LUT-based DDFTN at the threshold of 3.8×10^{-3}. However, a penalty of more than 1 dB arises after 2 km SSMF compared with the BTB scenario. In contrast with the high ROP situation, the original DDFTN scheme exhibits less performance improvement at low ROP. However, the LUT-based DDFTN algorithm shows an approximately 2 dB improvement compared with the FFE-only algorithm. It also shows an evident performance improvement in with the original DDFTN, as shown in Figure 7a. When the memory length becomes longer, the value of the BER continues to decrease. In a high-speed system, there is more severe ISI, which indicates that more symbols are involved. As a consequence, the LUT-based DDFTN algorithm, which takes more symbols into consideration, treats the ISI more closely to the actual condition. However, it introduces higher computational complexity, which limits its implementation. This tradeoff between performance and complexity is an important topic to consider.

In Figure 7b, the FFE-only algorithm fails to recover the distorted signal due to the severe dispersion and insufficient digital signal process, while DDFTN is able to achieve the HD-FEC threshold. Simultaneously, the LUT-based DDFTN with a 5-symbol pattern shows a >1 dB performance improvement compared with the original DDFTN. When the bit rate is at 140 Gbit/s, regardless of whether they are under BTB or the 1 km SSMF transmission, LUT-based DDFTN schemes always outperform the other schemes. As the pattern length increases from 3 to 5, the LUT-based DDFTN with the 5-symbol pattern also shows performance improvement. However, considering the system performance and computational complexity, a LUT-based DDFTN with a 3-symbol pattern may be preferred.

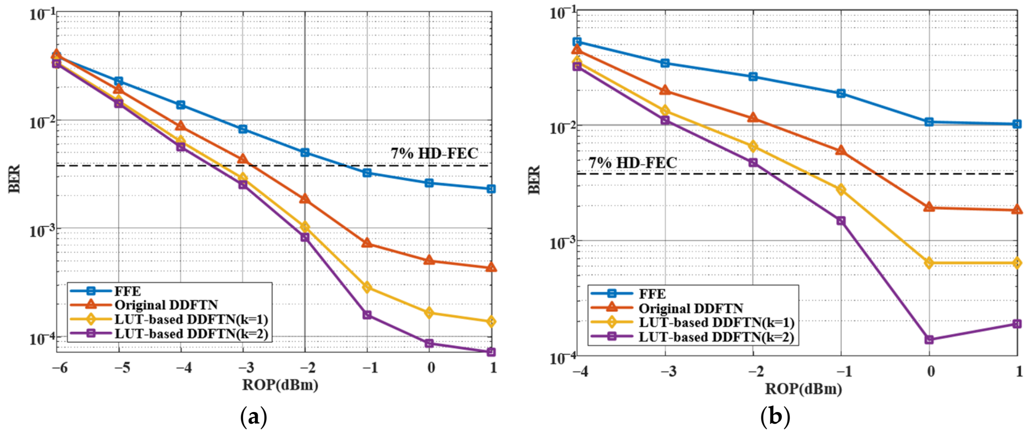

Figure 7. BER versus ROP for the 140 Gbit/s PAM-4 for (**a**) BTB; (**b**) 1 km SSMF.

To further investigate the performance of the LUT-based DDFTN algorithm, an LS-based DDFTN algorithm with a different memory length is considered to compare the performance, as shown in Figure 8. Solutions based on LS channel estimation and a LUT with a 3-symbol pattern can show similar performances. Nevertheless, a LUT-based DDFTN with a 5-symbol pattern performs better at high ROP, especially in the 140 Gbit/s system. It always has the edge when ROP changes from −2 dBm to 1 dBm. As shown in Table 1, although the ROP is almost identical at the BER of 3.8×10^{-3}, the high complexity based on the LS channel estimation has limited its implementation. The proposed LUT-based DDFTN algorithm effectively reduces the computational complexity and maintains a similar or better performance to the LS-based DDFTN algorithm.

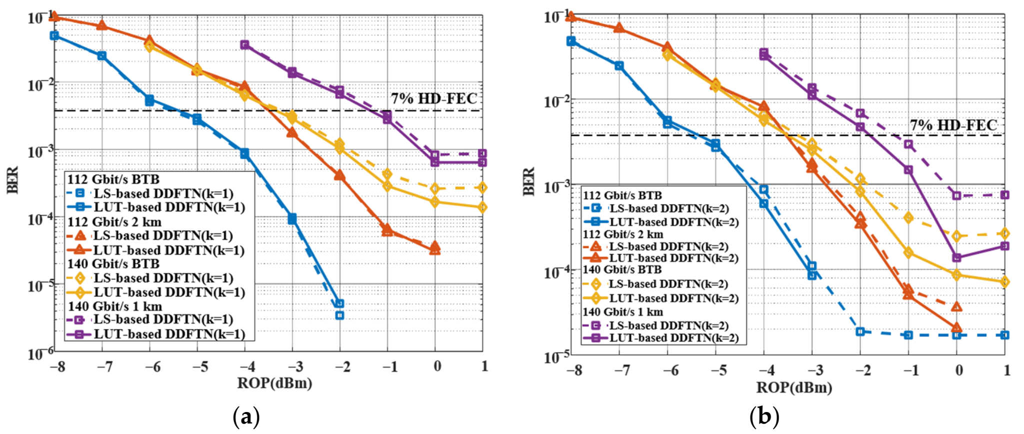

Figure 8. BER versus ROP for the LS-based and LUT-based DDFTN algorithms for a (**a**) 3-symbol pattern; (**b**) 5-symbol pattern.

5. Conclusions

In this work, we propose a LUT-based DDFTN algorithm to mitigate the pattern-dependent distortion. The error table generated by the LUT algorithm is introduced to obtain the estimated symbol in the DDFTN. Focused on the performance of the PAM-4 IM/DD system that suffers from severe bandwidth limitation and fiber dispersion, the original DDFTN, LS-based DDFTN, and LUT-based DDFTN algorithms are utilized to mitigate the pattern-dependent distortion. The impact of memory length is also considered at different rates and distances. We experimentally demonstrate the IM/DD transmission based on the PAM-4 signal. The experimental results show that the LUT-based DDFTN shows a >1 dB performance improvement compared with the original DDFTN in the 140 Gbit/s PAM-4 signal transportation under 1 km SSMF. Furthermore, whether under BTB or 1 km SSMF, LUT-based DDFTN schemes always outperform other schemes when the bit rate is at 140 Gbit/s. Enabled by the LUT-based DDFTN, the transmission of the PAM-4 signal is successfully achieved with a BER below the HD-FEC threshold of 3.8×10^{-3}. The LUT-based DDFTN scheme presents superiority in compensating for the pattern-dependent distortion. Compared to the LS-based DDFTN algorithm, the LUT-based DDFTN algorithm shows an approximately equivalent performance with low computational complexity.

Author Contributions: Conceptualization, K.L. and W.H.; methodology, X.Z., J.H., S.L., W.H. and K.L.; software, X.Z., J.H. and S.L.; validation, X.Z., J.H. and S.L.; writing—original draft preparation, X.Z.; writing—review and editing, all authors contributed equally. All authors have read and agreed to the published version of the manuscript.

Funding: This research was funded by the National Key Research and Development Program of China 2021YFB2900801, the National Natural Science Foundation of China NSFC, 62201033, U22A2005, the Young Elite Scientists Sponsorship Program of CIC 2021QNRC001, the Guangdong Basic and Applied Basic Research Foundation (2020A1515111047), and the Foundation of the Beijing Engineering and Technology Center for Convergence Networks and Ubiquitous Services.

Institutional Review Board Statement: Not applicable.

Informed Consent Statement: Not applicable.

Data Availability Statement: The datasets generated and analyzed during the current study are available from the corresponding author on reasonable request.

Conflicts of Interest: The authors declare no conflict of interest.

References

1. Ozolins, O.; Joharifar, M.; Salgals, T.; Louchet, H.; Schatz, R.; Gruen, M.; Dippon, T.; Kruger, B.; Pittala, F.; Che, D.; et al. Optical Amplification-Free High Baud rate Links for Intra-Data Center Communications. *J. Light. Technol.* **2023**, *41*, 1200–1206. [CrossRef]
2. Wang, W.; Li, H.; Zhao, P.; Zhang, Z.; Zang, D.; Wang, C.; Li, L.; Ma, L.; Liu, Y.; Zhu, N.; et al. Advanced Digital Signal Processing for Reach Extension and Performance Enhancement of 112 Gbps and Beyond Direct Detected DML-Based Transmission. *J. Light. Technol.* **2019**, *37*, 163–169. [CrossRef]
3. Huo, J.; Zhou, X.; Shang, C.; Huangfu, W.; Yuan, J.; Ning, H.; Long, K.; Yu, C.; Lau, A.P.T.; Lu, C. Theoretical and Numerical Analyses for PDM-IM Signals Using Stokes Vector Receivers. *Sci. China Inf. Sci.* **2020**, *63*, 202307. [CrossRef]
4. Xiang, M.; Fu, S.; Xu, O.; Li, J.; Peng, D.; Gao, Z.; Wang, Y.; Qin, Y. Advanced DSP Enabled C-Band 112 Gbit/s/λ PAM-4 Transmissions with Severe Bandwidth-Constraint. *J. Light. Technol.* **2022**, *40*, 987–996. [CrossRef]
5. Tang, X.; Qiao, Y.; Chen, Y.-W.; Lu, Y.; Chang, G.-K. Digital Pre- and Post-Equalization for C-Band 112-Gb/s PAM4 Short-Reach Transport Systems. *J. Light. Technol.* **2020**, *38*, 4683–4690. [CrossRef]
6. Moon, S.-R.; Kang, H.-S.; Rha, H.Y.; Lee, J.K. C-Band PAM-4 Signal Transmission Using Soft-Output MLSE and LDPC Code. *Opt. Express* **2019**, *27*, 110. [CrossRef] [PubMed]
7. Man, J.; Fu, S.; Chen, W.; Gao, J.; Liu, X.; Zeng, L. 25-Gb/s and 40-Gb/s faster-than-nyquist PON based on low-cost 10G-class optics. In Proceedings of the Asia Communications and Photonics Conference (ACP), Hong Kong, China, 19–23 November 2015.
8. Chen, C.; Tang, X.; Zhang, Z. Transmission of 56-Gb/s PAM-4 over 26-Km Single Mode Fiber Using Maximum Likelihood Sequence Estimation. In Proceedings of the 2015 Optical Fiber Communications Conference and Exhibition (OFC), Los Angeles, CA, USA, 22–26 March 2015.
9. Zhong, K.; Chen, W.; Sui, Q.; Man, J.; Lau, A.P.T.; Lu, C.; Zeng, L. Experimental Demonstration of 500Gbit/s Short Reach Transmission Employing PAM4 Signal and Direct Detection with 25Gbps Device. In Proceedings of the 2015 Optical Fiber Communications Conference and Exhibition (OFC), Los Angeles, CA, USA, 22–26 March 2015.
10. Li, X.; Faruk, S.; Savory, S.J. Advanced Nonlinear Digital Signal Processing for Short-Reach Applications. In Proceedings of the Optical Fiber Communication Conference (OFC) 2021, San Francisco, CA, USA, 6–10 June 2021; p. F2D.3.
11. Zhang, D.; Wang, S.; He, P.; Zhang, M.; Liu, D. Joint FFE and Error-Based-FFE Algorithm for 100 Gb/s Bandwidth-Limited IMDD Optical System. In Proceedings of the 2022 Asia Communications and Photonics Conference (ACP), Shenzhen, China, 5 November 2022; IEEE: Piscataway, NJ, USA, 2022; pp. 733–736.
12. Yu, Y.; Che, Y.; Bo, T.; Kim, D.; Kim, H. Reduced-State MLSE for an IM/DD System Using PAM Modulation. *Opt. Express* **2020**, *28*, 38505. [CrossRef] [PubMed]
13. Zhong, K.; Zhou, X.; Gao, Y.; Chen, W.; Man, J.; Zeng, L.; Lau, A.P.T.; Lu, C. 140-Gb/s 20-Km Transmission of PAM-4 Signal at 1.3μm for Short Reach Communications. *IEEE Photonic Technol. Lett.* **2015**, *27*, 1757–1760. [CrossRef]
14. Hussein, Y.S.; Alias, M.Y.; Abdulkafi, A.A. On Performance Analysis of LS and MMSE for Channel Estimation in VLC Systems. In Proceedings of the 2016 IEEE 12th International Colloquium on Signal Processing & Its Applications (CSPA), Melaka, Malaysia, 4–6 March 2016.

15. Munshi, A.; Unnikrishnan, S. Performance Analysis of Compressive Sensing Based LS and MMSE Channel Estimation Algorithm. *J. Syst. Softw.* **2021**, *17*, 13–19. [CrossRef]
16. Huo, J.; Liu, S.; Shang, C.; Zhang, X.; Huangfu, W.; Long, K. Modified DDFTN Algorithm for Band-Limited Short-Reach Optical Interconnects. *J. Light. Technol.* **2023**, 1–7. [CrossRef]
17. Zhou, J.; Bai, L.; Liu, Q.; Hu, S.; Zhu, M.; Zhang, J.; Qiu, K. Performance and Complexity Comparison of Different Equalizers in 100-Gb/s PAM-4 Signal Transmission Systems. In Proceedings of the Asia Communications and Photonics Conference 2021, Shanghai, China, 24–27 October 2021; p. T4A.94.
18. Zhang, J.; Gou, P.; Kong, M.; Fang, K.; Xiao, J.; Zhang, Q.; Xin, X.; Yu, J. PAM-8 IM/DD Transmission Based on Modified Lookup Table Nonlinear Predistortion. *IEEE Photonics J.* **2018**, *10*, 7903709. [CrossRef]
19. He, Z.; Vijayan, K.; Mazur, M.; Karlsson, M.; Schroder, J. Look-up Table Based Pre-Distortion for Transmitters Employing High-Spectral-Efficiency Modulation Formats. In Proceedings of the 2020 European Conference on Optical Communications (ECOC), Brussels, Belgium, 6–10 December 2020; IEEE: Piscataway, NJ, USA, 2020.
20. Huo, J.; Zhou, X.; Zhong, K.; Guo, C.; Yuan, J.; Tu, J.; Long, K.; Tao Lau, A.P.; Lu, C. Experimental Demonstration of Novel ETC Algorithm for 112 Gbit/s PAM-4 Signals Transmission Over 40km without Optical Amplifier. In Proceedings of the 2018 European Conference on Optical Communication (ECOC), Rome, Italy, 23–27 September 2018; IEEE: Piscataway, NJ, USA, 2018.
21. Chen, Z.; Dai, X.; Nie, J.; Zhang, S.; Zhou, J.; Zhang, J.; Luo, M.; Yang, Q.; Deng, L.; Cheng, M.; et al. Compressed Look-up Table-Based Implementation Friendly MLSE Equalizer for C-Band DSB IM/DD Transmission. In Proceedings of the 2022 European Conference on Optical Communication (ECOC), Basel, Switzerland, 18–22 September 2022.
22. Gou, P.; Zhao, L.; Wang, K.; Zhou, W.; Yu, J. Nonlinear Look-Up Table Predistortion and Chromatic Dispersion Precompensation for IM/DD PAM-4 Transmission. *IEEE Photonics J.* **2017**, *9*, 1–7. [CrossRef]
23. Zhang, J.; Yu, J.; Chien, H.-C. EML-Based IM/DD 400G (4 $\times$ 112.5-Gbit/s) PAM-4 over 80 Km SSMF Based on Linear Pre-Equalization and Nonlinear LUT Pre-Distortion for Inter-DCI Applications. In Proceedings of the 2017 Optical Fiber Communications Conference and Exhibition (OFC), Los Angeles, CA, USA, 19–23 March 2017.
24. Zhou, J.; Zhang, J.; Zhao, X.; Jiang, W.; Hu, S.; Zhu, M.; Qiu, K. Simplified TC-MLSE Equalizer for 210-Gb/s PAM-8 Signal Transmission in IM/DD Systems. In Proceedings of the Optical Fiber Communication Conference (OFC) 2022, San Diego, CA, USA, 6–10 March 2022.
25. Zhou, J.; Zhang, J.; Zhao, X.; Jin, T.; Hu, S.; Lin, H.; Yu, Z.; Zhang, Q.; Xu, B.; Qiu, K. Advanced Nonlinearity Equalizer with TC-NL-MLSE for Transmitting beyond 200-Gb/s PAM-8 in IM/DD Systems. *Opt. Express* **2022**, *30*, 37416. [CrossRef]